



Stimulation of ambient energy generated electric field on crop plant growth

Xunjia Li^{1,2}, Jianjun Luo^{1,3} , Kai Han^{1,3} , Xue Shi^{1,3}, Zewei Ren^{1,3}, Yi Xi⁴, Yibin Ying², Jianfeng Ping²  and Zhong Lin Wang^{1,3,5} 

Eco-friendly technologies are of great significance to agricultural sustainability due to the environmental damage caused by agricultural activities. Here, we report a wind and rain energy-driven electrical stimulation system for enhancing crop production. The system is based on an all-weather triboelectric nanogenerator (AW-TENG), which is composed of a bearing-and-hair structured triboelectric nanogenerator (TENG) and a raindrop-driven TENG. Treated by the self-generated high-voltage electric field, the system can increase pea seeds germination speed by ~26.3% and pea yield by ~17.9%. By harvesting environmental wind and raindrop energy, the AW-TENG can be used to drive various agricultural sensors for optimizing plant growth. This work provides a fresh direction for self-powered systems in safe, efficient and eco-friendly agricultural production improvement and may profoundly contribute to the construction of a sustainable economy.

The chemical revolution of agriculture in the twentieth century dramatically increased crop yields and alleviated global food shortages^{1–3}. However, the misuse of chemical fertilizers and pesticides imposes an enormous burden on the environment and human health^{4,5}. Therefore, there is a need to develop new yield-enhancing technologies to help conventional agriculture reduce its dependence on agrochemicals while maximizing sustainable growth in agricultural yields⁶. Relevant studies revealed that external high electrostatic field can not only be used to accelerate seed germination and plant growth^{7,8} but also improve ion migration in the soil for better nutrient absorption⁹. However, the commercial voltage boosting methods generally need an external power supply and have considerable limitations, such as complex circuits, high installation costs and shock hazard. To achieve sustainable social development, it is necessary to develop an efficient, maintenance-free and eco-friendly technology to increase agricultural production.

In recent years, originated from the coupling effect of contact electrification and electrostatic induction, triboelectric nanogenerator (TENG) has risen strongly in the field of renewable energy^{10,11}. With advantages of high output voltage, low cost, light weight and wide material selectivity, TENGs can collect various kinds of mechanical energy from the external environment for realizing self-powered electronics networks on a large scale. The applications of TENG have infiltrated many aspects of our daily life, including micro/nano power source^{12,13}, self-powered sensors^{14–16} and blue energy^{13,17,18}. Besides, given that the inherent output characteristics of high voltage and low current, TENG can also be used as a direct power source for driving many high-voltage applications such as electrospinning¹⁹, dielectric wetting²⁰, air negative ions releasing²¹ and so on. Compared with traditional high-voltage power sources, TENG-based high-voltage power sources have unique advantages of safety, cost-effectiveness and portability. Therefore, establishing a

low-cost, safe and reliable crop production promotion system based on TENG technology holds promise.

Here, we propose a self-powered electrical stimulation system (SESS) for enhancing agricultural production based on the all-weather TENG (AW-TENG) integrated by a bearing-and-hair structured TENG (BH-TENG) and a raindrop-driven TENG (R-TENG). With the bearing spacer, hair brush and all-in-one structure design, the AW-TENG is capable of harvesting wind and raindrop energy efficiently. Benefiting from its high-voltage output performance, the AW-TENG can be directly used to stimulate plant growth, with remarkable increases of ~26.3% and ~17.9% in pea germination speed and yield. The mechanism for crop growth promotion is also systematically investigated by measuring multiple physical and chemical indexes. Furthermore, by harvesting environmental energy such as wind and raindrops, the AW-TENG can be used to construct a self-powered agricultural monitoring system, which is beneficial for plant growth strategy optimization and management. This work demonstrates an innovative concept of a SESS for plant growth, which will have great application potential in future agriculture.

Results

Self-powered electrical stimulation system for crop growth.

In this work, we developed a prototype of SESS with low start-up conditions and high efficiency based on AW-TENG, which is composed of a BH-TENG and an R-TENG for harvesting environmental energy from wind and raindrop, respectively. Figure 1a depicts the SESS in the practical application scenario. By harvesting various kinds of environmental energy, the AW-TENG can not only directly stimulate crop growth with a high-voltage electric field but also drive agricultural sensors for optimizing crop growth strategies. The three-dimensional explosion diagram of the AW-TENG is shown in Fig. 1b, revealing its extremely high integration and space

¹CAS Center for Excellence in Nanoscience, Beijing Key Laboratory of Micro-nano Energy and Sensor, Beijing Institute of Nanoenergy and Nanosystems, Chinese Academy of Sciences, Beijing, China. ²College of Biosystems Engineering and Food Science, Zhejiang University, Hangzhou, China. ³School of Nanoscience and Technology, University of Chinese Academy of Sciences, Beijing, People's Republic of China. ⁴State Key Laboratory of Power Transmission Equipment & System Security and New Technology, Department of Applied Physics, School of Chemistry and Chemical Engineering, Chongqing University, Chongqing, China. ⁵School of Material Science and Engineering, Georgia Institute of Technology, Atlanta, GA, USA. ✉e-mail: luojianjun@binn.cas.cn; jfping@zju.edu.cn; zhong.wang@mse.gatech.edu

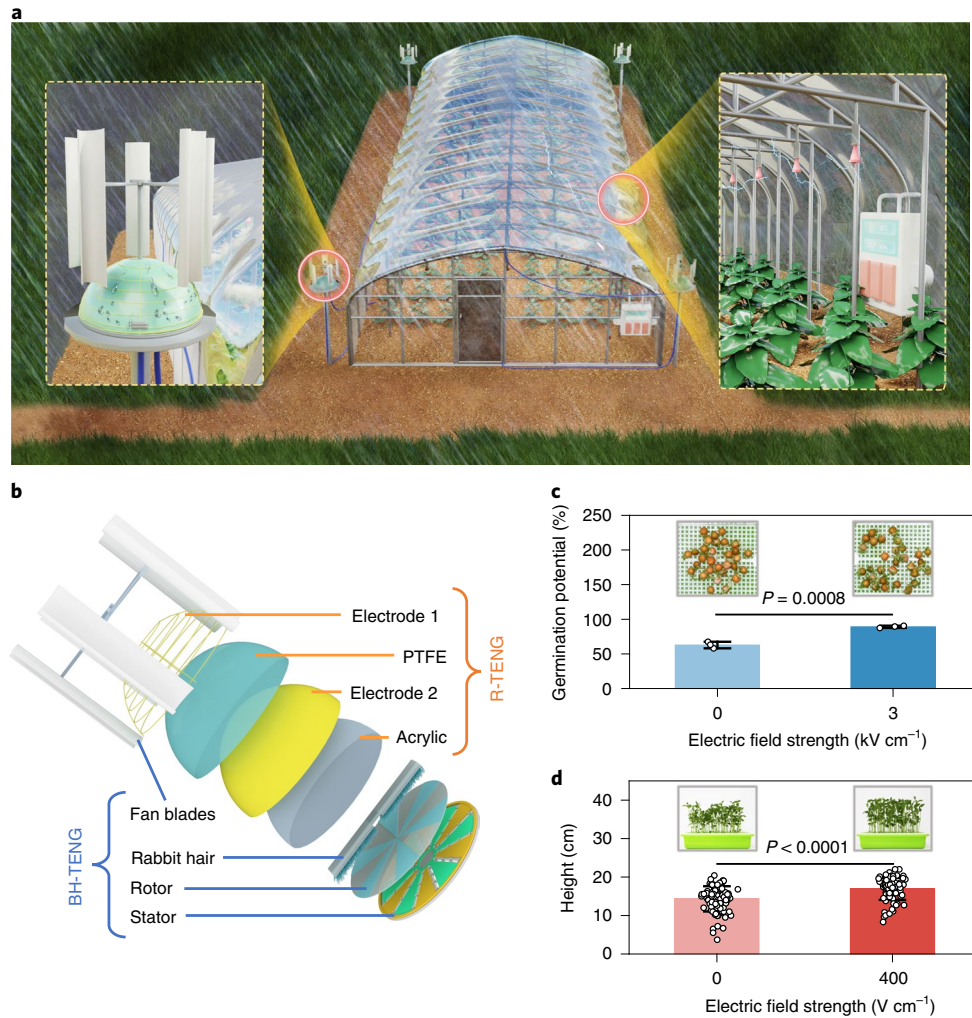


Fig. 1 | SESS for enhancing crop production. **a**, Schematic illustration of the SESS. The circled insets show the enlarged views of schematic diagrams of the AW-TENG and self-powered electric field array. **b**, Three-dimensional exploded view of the AW-TENG. **c,d**, The positive effect of the SESS on germination (**c**) and growth of peas (**d**). Values are means \pm s.d. (for **c**, $n = 3$ independent experimental groups, each group contained 95 independent seeds; for **d**, $n = 3$ independent experimental groups, each group contains 30 independent seedlings after 5 d of gemination). P values in **c** and **d** are based on two-tailed, two-sample t -tests and the detailed analyses are presented in Figs. 3c and 4d.

utilization. Covered by a waterproof acrylic shell, the BH-TENG is placed in the central position and consists of a stator, a rotor, rabbit hair and vertical-shaft blades connected to the rotor. The R-TENG is designed on the surface of the shell, including a copper electrode layer completely covered on the shell, an intermediate PTFE triboelectric layer and an outermost electrode array made of copper wire. For a photograph of the AW-TENG see Supplementary Fig. 1a. The self-powered electrostatic fields applying to crops or their seeds are generated by the AW-TENG and relevant experimental setups are shown in Supplementary Fig. 1b,c. Compared with untreated pea seeds, the germination potential of seeds treated with the self-powered electric field notably increased ($\sim 26.3\%$), which means that these seeds germinated faster (Fig. 1c). The growth rate of pea seedlings under the self-powered electric field also increased, with production up $\sim 17.9\%$ (Fig. 1d). These results preliminarily reveal the promoting effect of self-powered electrical stimulation on crop growth.

Structural design and output performance of the BH-TENG. With advantages of high voltage and good stability, rotating-disk TENGs are often used as the high-voltage power supply^{19,22–24}.

However, it is difficult for rotating-disk TENG to be driven by ambient wind due to the electrostatic adherence between stator and rotor caused by their high charge density. Besides, the violent friction of rotating-disk TENGs during the rotating process always generates wear of triboelectric layers, thus causing poor durability of TENG. Although introducing liquid lubrication to rotating-disk TENGs has been reported to reduce abrasion between triboelectric layers^{25,26}, the strong viscosity of lubricant will generate a large starting torque. To solve these problems, an innovative type of rotating-disk BH-TENG with high output, high stability, low wear and low starting torque was designed to efficiently harvest environmental wind energy (Fig. 2a). As a contrast, an original rotating-disk TENG and a rotating-disk TENG with bearing spacers (B-TENG) were designed (Supplementary Fig. 2a,b). It is evident that the addition of the bearing-and-rabbit hair structure can greatly improve the output performance while maintaining low friction (Fig. 2b,c). Compared with the traditional rotation-mode TENG, the starting torque of B-TENG and BH-TENG is only $\sim 1/12$ due to the decrease in electrostatic adherence. However, the increase of separation distance will weaken the electrostatic induction, causing poor output of B-TENG²⁷. By fixing rabbit hair with excellent flexibility, low

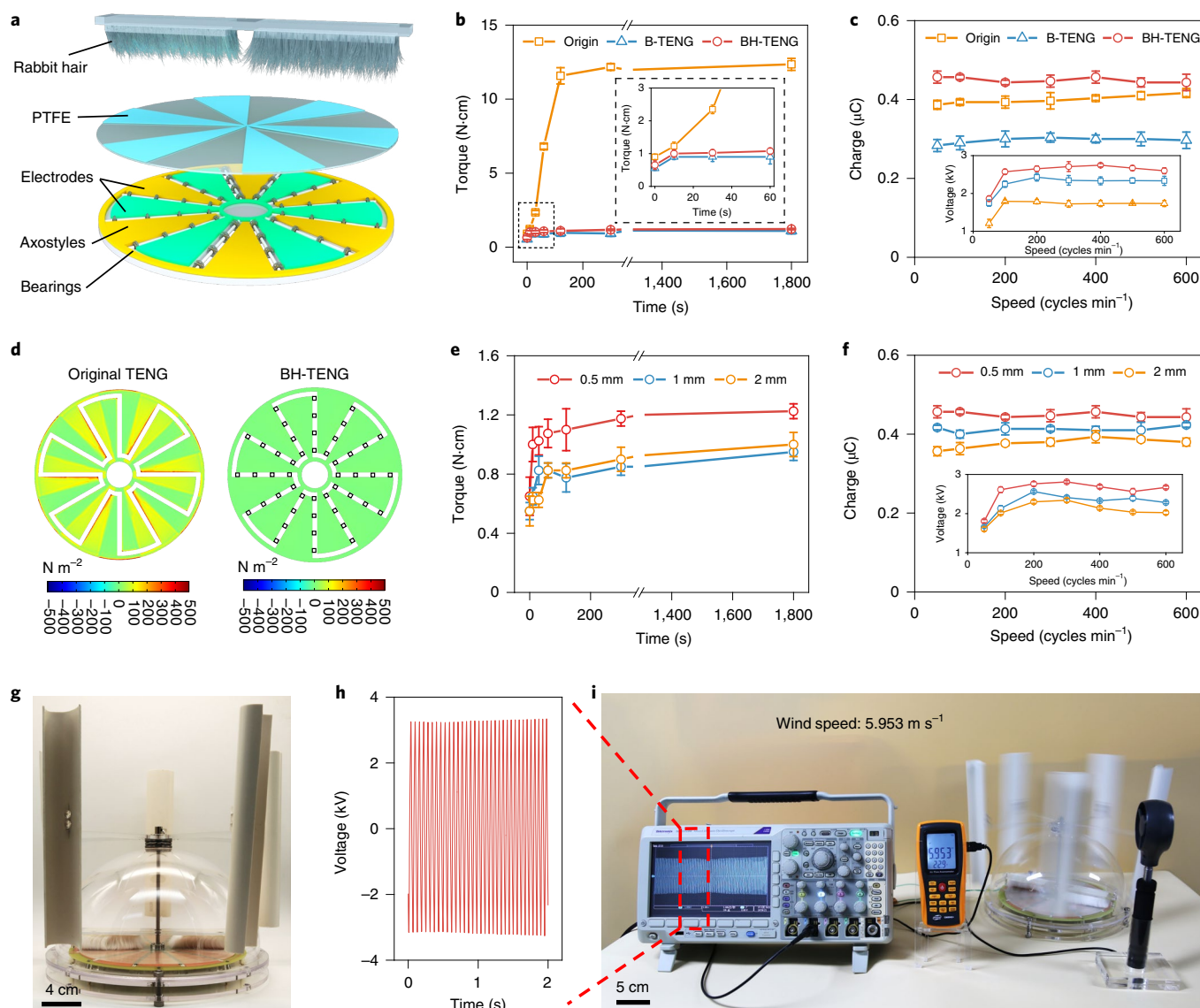


Fig. 2 | Structure and output performance of the BH-TENG. **a**, Structural design of the BH-TENG. **b**, Torque variation of the traditional rotation-mode TENG (Origin), B-TENG and BH-TENG with time running. The inset shows the torque variation of the traditional rotation-mode TENG (Origin), B-TENG and BH-TENG during 60 s. Values are means \pm s.d. ($n=3$ independent tests). Rotation speed was set as 400 r.p.m. and the gap height in BH-TENG and B-TENG was 0.5 mm. **c**, Maximum transferred charge of the traditional rotation-mode TENG (Origin), B-TENG and BH-TENG at different rotation speeds. The inset shows the output voltage of the traditional rotation-mode TENG (Origin), B-TENG and BH-TENG with bearing spacers of different heights. Values are means \pm s.d. ($n=3$ independent tests). **d**, Simulation of the Coulomb force distribution on rotors of traditional rotation-mode TENG and BH-TENG under the same surface charge density. **e, f**, Torque variation (**e**) and maximum transferred charge (**f**) of the BH-TENG with bearing spacers of different heights. The inset shows the output voltage of BH-TENG with bearing spacers of different heights. Values are means \pm s.d. ($n=3$ independent tests). **g**, A photograph of BH-TENG. **h, i**, Output voltage and operation status of BH-TENG under the wind speed of 5.953 m s^{-1} . Ambient relative humidity was set as $\sim 40\%$ and the gap height in BH-TENG was 0.5 mm. The wind was induced by an air blower and the distance between the air blower and BH-TENG was $\sim 1 \text{ m}$.

density, high hair density and rich protein on the top of the rotor in BH-TENG as a friction excitation material²⁸, the output charges can be continuously replenished and even higher than that of the traditional rotation-mode TENG. The detailed output voltage of the traditional rotation-mode TENG, B-TENG and BH-TENG under different wind speeds is shown in Supplementary Fig. 3. Similarly, the output power and current of the traditional rotation-mode TENG, B-TENG and BH-TENG also show similar trends (Supplementary Fig. 4). Moreover, due to the existence of an external protective case, BH-TENG has good sealing and can maintain an excellent output

in high-humidity environments (Supplementary Fig. 5). The output stability of the BH-TENG can also be greatly enhanced through this structural design (Supplementary Fig. 6). It is worth noting that the BH-TENG can reach charge saturation state within 10 s of start-up (Supplementary Fig. 7) and is more suitable for practical scenarios.

To further verify the effect of bearing spacers on the Coulomb force and output, COMSOL software was used to simulate the Coulomb force and potential distribution on the rotor surfaces of the traditional rotation-mode TENG and BH-TENG. The Coulomb force on the rotor surface of BH-TENG is much smaller than that of

the traditional rotation-mode TENG under the same condition of charge density, while the surface potential hardly decreases (Fig. 2d and Supplementary Fig. 8), which is consistent with previous experimental results. Subsequently, the influence of bearing spacer height on starting torque and output of BH-TENG was also studied. As shown in Fig. 2e, the starting torque of BH-TENG decreases as the height of the bearing spacer increases, which conforms to the calculation formula of Coulomb force. Similarly, the output of BH-TENG at different wind speeds is also inversely proportional to the height of the bearing spacer (Fig. 2f). The output stability of the BH-TENG with bearing spacers of different heights is shown in Supplementary Fig. 9. Figure 2g exhibits the photograph of the BH-TENG device, including the vertical-shaft fan blade and the protective casing. The detailed structure of the stator with bearing spacers is shown in Supplementary Fig. 10a,b. Thanks to the addition of bearing spacers and rabbit hair, BH-TENG can output a high voltage exceeding 3 kV under the simulated natural wind, while the traditional rotation-mode TENG cannot work at a similar wind speed (Fig. 2h,i and Supplementary Fig. 11a). Besides, compared with the traditional rotation-mode TENG with a start-up wind speed of 6 m s^{-1} , BH-TENG can output stably under an ultralow wind speed of 0.5 m s^{-1} (Supplementary Fig. 11b,c). The detailed rotation situations of the traditional rotation-mode TENG and BH-TENG under the simulated natural wind are shown in Supplementary Videos 1 and 2.

The germination-promoting effect of the SESS. In agricultural production, germination rate and germination speed are two important indicators to characterize the quality of crop seeds^{29–31}. In previous work, the germination speed and yield of seeds screened by electrostatic separators were remarkably increased³² and further studies reveal a beneficial effect of electric field on the physiological activities and insect resistance of seeds^{33,34}. In this study, AW-TENG was used as a high-voltage power supply of the self-powered electric field to modulate the germination of pea seeds. As shown in Fig. 3a, pea seeds are directly placed on the lower plate connected to the negative electrode and the upper plate is connected to the positive electrode to fix the direction of the self-powered electric field. The electric field intensity change is realized by adjusting the distance between the upper and lower plates. The seeds treated with electric fields of different intensities were placed in the darkroom for germination. After 1 day of germination, some seeds grew roots but no seeds germinated. The difference in germination number became apparent after 3 days of germination and the germination rate of pea seeds treated with a 2 kV cm^{-1} electric field is 41.2% higher than that of the control group (Fig. 3b and Supplementary Fig. 12). Five days later, almost all of the seeds in each group were germinated, except for the devitalized seeds and the growth rate of the seeds treated with electric field was remarkably higher than that of the untreated ones. The germination details of each group of seeds in the parallel experiment are shown in Supplementary Fig. 13. To quantify the effect of the self-powered electric field on seeds, some parameters related to seed germination were measured. Consistent with the pea seeds germination status, the calculated germination potential and germination index of the seeds after electric field treatment is higher than that of untreated seeds by as much as 26.3% and 30%, respectively (Fig. 3c,d). However, the higher field strength of 3 kV cm^{-1} does not seem to further improve the germination rate and speed, which may be attributed to the limited response of seeds to electric field intensity. The vigour index of pea seeds also follows this trend, which further exhibits the promoting effect on seed germination of the as-designed self-powered electric field (Fig. 3e). Moreover, the seedling heights and root lengths of pea seeds treated with different intensity electric fields after 5 days of growth were also counted. Up to 13.7% improvement in seedling length and root length of peas was observed when treated by a 2 kV cm^{-1} electric field (Fig. 3f,g and Supplementary Fig. 14a). The weight of peas treated by the elec-

tric field also increased to a certain extent compared to untreated peas, with a notable difference of $\sim 14.4\%$ (Supplementary Fig. 14b). To exclude and verify environmental factors on seed growth characteristics, we studied the growth states of seeds under different humidities and temperatures. The germination rate, vigour index, seedling height and weight of seeds treated with electric field were all enhanced compared to the untreated ones under relative ambient humidities of 30% and 90% (Supplementary Figs. 15 and 16). As shown in Supplementary Figs. 17 and 18, the treated seeds also showed better growth performance at 35°C . Although none of the seeds germinated at 15°C within 5 days since low temperature remarkably slows seed germination, the roots of peas still grew better when treated with the electric field. These results reveal that the pretreatment of a self-powered electric field can notably promote the germination and growth of pea seeds.

To explore the stimulation mechanism of the self-powered electric field on seed germination, we analysed the soluble protein content, respiration intensity, peroxidase (POD) activity and malondialdehyde (MDA) content, which are related to the strength of plant life activities and total plant metabolism^{35,36}. First, the Coomassie Brilliant Blue staining method was used to determine the content of soluble protein in seeds after the third day of germination³⁷. The soluble protein content of pea seeds was calculated according to the standard curves and the content of pea seeds treated with an electric field strength of 2 kV cm^{-1} is $\sim 13\%$ higher than that of pea seeds without electric field treatment (Supplementary Fig. 19a,b). Similarly, there was a notable difference in the respiration intensity of the seeds treated with a 2 kV cm^{-1} electric field and the untreated group ($\sim 29.9\%$) (Supplementary Fig. 19c), which reveals the metabolism-enhancing activity of the self-powered electric field on plant seeds. The POD activity of pea seeds treated with the electric field was also higher than that of untreated ones ($\sim 26.8\%$), showing the enhanced repair capacity of the membrane system by the electric field (Supplementary Fig. 20a). Moreover, the MDA content of the treated seeds was also remarkably lower than that of the control group, demonstrating the mitigating effect of electric field on the cellular peroxidation within the seeds, which may be attributed to the enhanced activity of the intracellular oxygen radical scavenging enzyme system (Supplementary Fig. 20b). To verify the universal promoting effect of the self-powered electric field on crop plant growth, other types of plant seeds (Chinese cabbage and soybean) were selected for statistical analysis. As shown in Supplementary Figs. 21 and 22, the daily germination rate and vigour index of Chinese cabbage and soybean seeds treated with the electric field of 2 kV cm^{-1} exceeded those of untreated ones. In addition, the seedling height and weight of treated seeds were about 20% higher than those of the control group, indicating that the self-powered electric field has a facilitating effect on the germination for these two kinds of seeds.

The growth-promoting effect of the SESS. In addition to the acceleration of seed germination, the growth-promoting effect of the electric field on plant seedlings is also demonstrated^{8,38}. Thus, the AW-TENG-driven self-powered electric field for crop seedling growth promotion was designed as shown in Fig. 4a. The assumption of the detailed effect of the self-powered electric field on the crop seedling is shown in Fig. 4b. The positive effect of the self-powered electric field on crop yield was exhibited by measuring the detailed growth parameters of pea seedlings under the electric fields with different intensities. After 7 days of growth, the average height of pea seedlings under the self-powered electric field is notably higher than that of the control group, with a maximum difference of up to 17.9% (Fig. 4c). Likewise, the average root lengths of these seedlings show a similar trend (Supplementary Fig. 23). The detailed growth situations of pea seedlings under different field strengths within 5 days are shown in Supplementary Fig. 24. The daily height

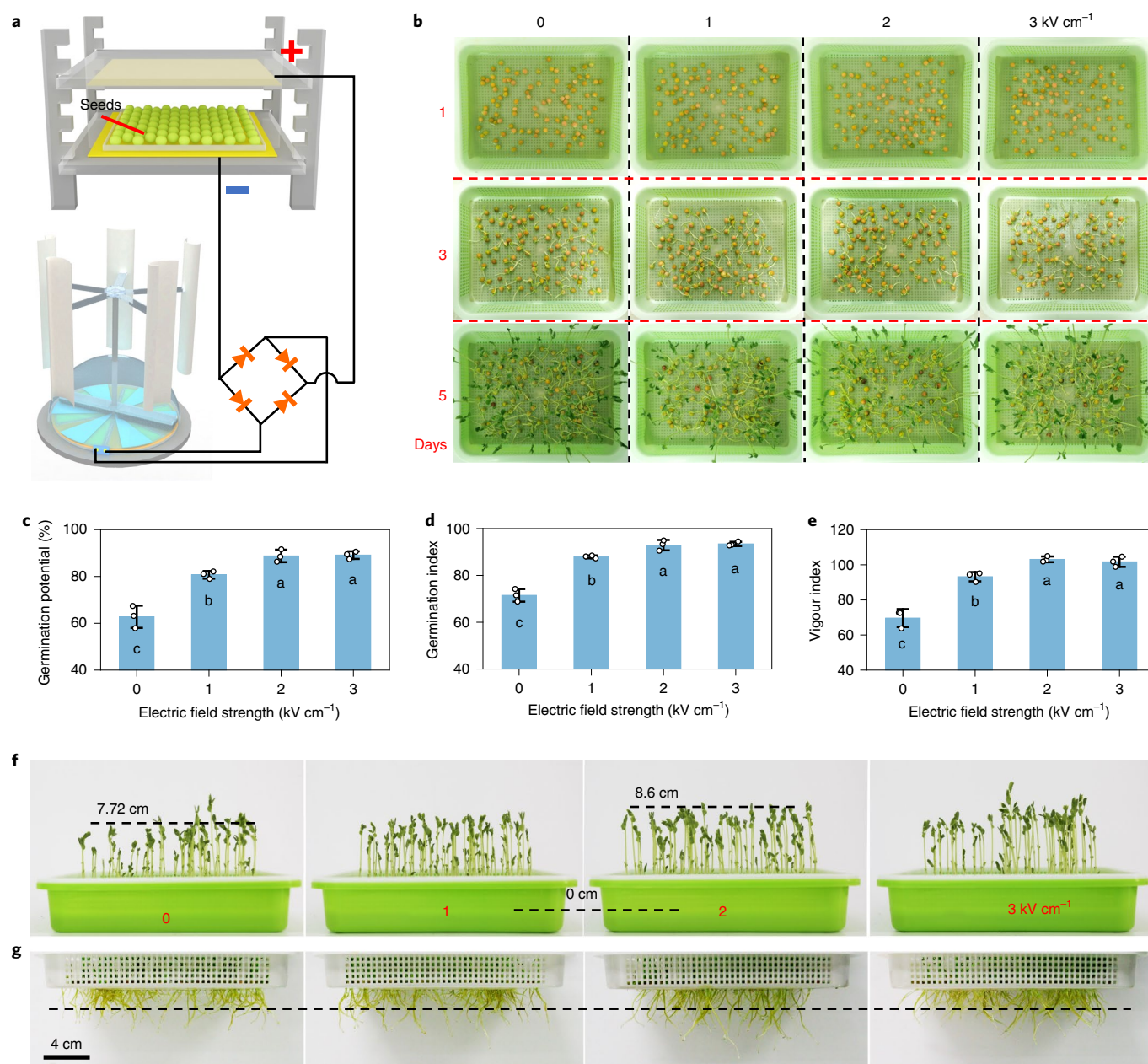


Fig. 3 | Germination promotion of the SESS. **a**, Schematic representation of the self-powered electric field for seed treatment, including an AW-TENG, a rectifier circuit and a parallel electric field generator. **b**, Germination status of peas within 5 d. **c–e**, Germination potential (**c**), germination index (**d**) and vigour index (**e**) of the pea seeds treated with the self-powered electric field of different strengths after 5 d of germination. Values are means \pm s.d. ($n=3$ independent experimental groups; each group contained 95 independent seeds; their calculation refers to Supplementary Notes 1, 2 and 3). **f, g**, Photographs of the stems (**f**) and roots (**g**) of the peas treated with the self-powered electric field of different strengths after 5 d of germination. Different letters in bars indicate a significant difference at $P < 0.05$. The P value in **c** versus the 0 kV cm^{-1} for 1 kV cm^{-1} is 7.3×10^{-5} , for 2 kV cm^{-1} is 5×10^{-6} and for 3 kV cm^{-1} is 4×10^{-6} . The P value in **d** versus the 0 kV cm^{-1} for 1 kV cm^{-1} is 4×10^{-6} , for 2 kV cm^{-1} is 5.4×10^{-7} and for 3 kV cm^{-1} is 4.5×10^{-7} . The P value in **e** versus the 0 kV cm^{-1} for 1 kV cm^{-1} is 2.3×10^{-5} , for 2 kV cm^{-1} is 2×10^{-6} and for 3 kV cm^{-1} is 2×10^{-6} . The data in **c**, **d** and **e** were analysed by ANOVA one-way comparison followed by LSD test. The germination of seeds was performed in a darkroom and the ambient temperature and relative humidity were maintained at 25°C and 60% by using an air conditioner and humidifier.

statistical results of pea seedlings reflect the remarkable gap between the height of pea seedlings with or without the electric field treatment (Fig. 4d). Moreover, after growing for 7 days, the average weight of the seedlings under the electric field was $\sim 20.3\%$ higher than that of the untreated ones (Supplementary Fig. 25).

The notable positive effect of self-powered electric field on the growth of pea seedlings may arise from the continuous effect of the self-powered electric field on the photosynthesis⁵. To verify

this stimulation mechanism, chlorophyll content and fluorescence analysis were used to characterize the photosynthesis of pea seedlings. Soil and plant analysis development (SPAD) value can be used to quickly and easily characterize the chlorophyll content of plants and there is a positive correlation between SPAD value and photosynthesis intensity of plants^{39–41}. Accompanied by a continuous rise in the difference of SPAD values between pea seedlings under electric fields with different strengths during 7 days, the difference

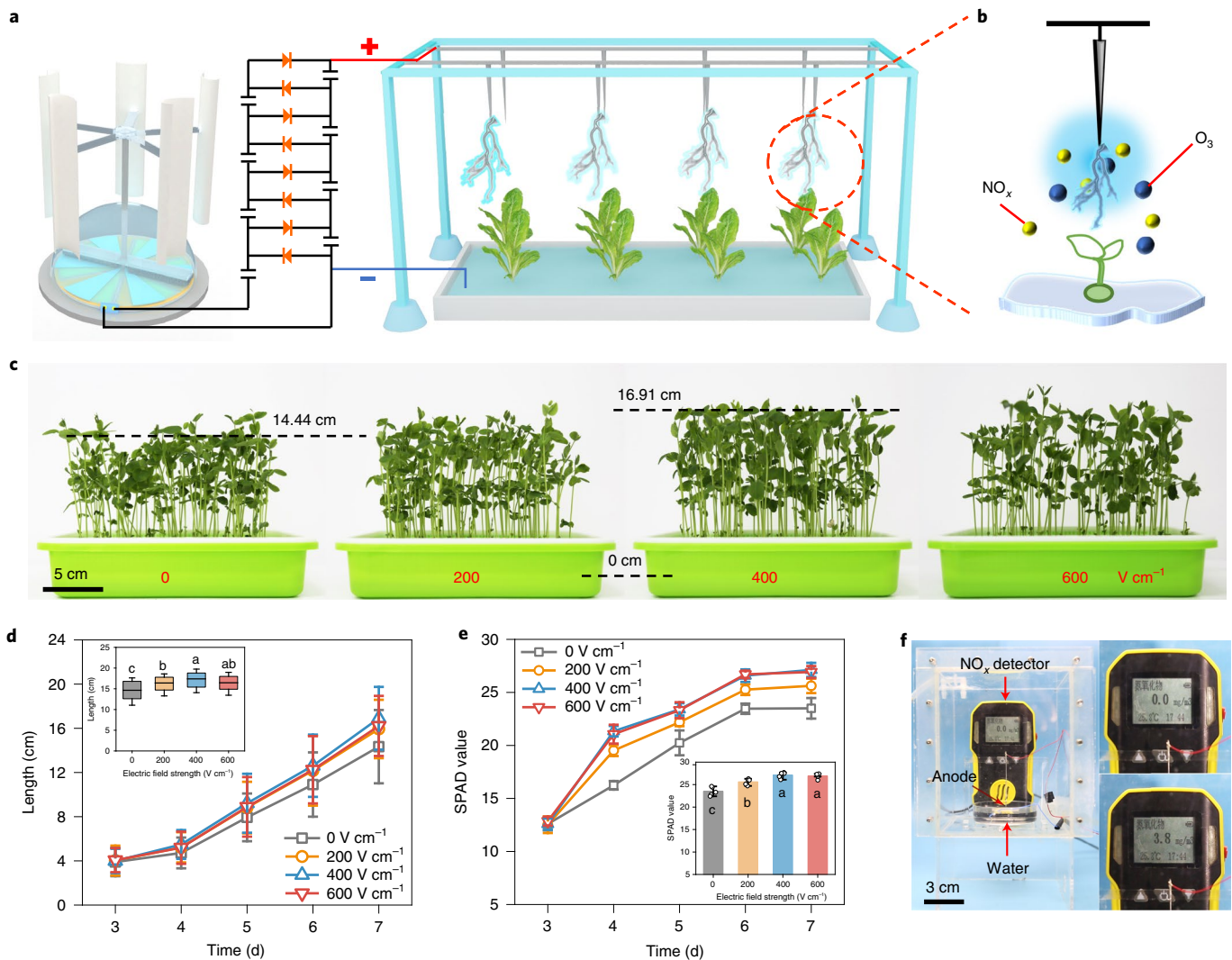


Fig. 4 | Growth acceleration of the SESS. **a**, A diagram of the self-powered electric field for pea seedlings treatment, including an AW-TENG, a voltage multiplier circuit and a discharge device. **b**, Schematic diagram of the principle of self-powered electric field affecting plant growth. **c**, Photos of the pea seedlings treated with the self-powered electric field of different strengths for 5 d. The light for the plants was provided by full-spectrum LEDs with a strength of 4,000 lux for 14 h every day and the ambient temperature and relative humidity were maintained at 25 °C and 60% by using an air conditioner and humidifier. **d**, Stem heights of the pea seedlings treated with the self-powered electric field of different strengths for different days. Inset: stem heights of the pea seedlings treated with the self-powered electric field of different strengths for 7 d. The box plots show median (solid line), 25th and 75th percentile (top and bottom of boxes) and s.d. (whiskers). Values are means \pm s.d. ($n=3$ independent experimental groups; each group contains 30 independent seedlings). Different letters in bars indicate a significant difference at $P < 0.05$. The P value in inset versus the 0 V cm^{-1} for 200 V cm^{-1} is 2.4×10^{-4} , for 400 V cm^{-1} is 6.2×10^{-9} and for 600 V cm^{-1} is 1.8×10^{-5} . **e**, SPAD value of the pea seedlings treated with the self-powered electric field of different strengths for different days. Values are means \pm s.d. ($n=5$ independent leaves; the measurement refers to Supplementary Note 8). Different letters in bars indicate a significant difference at $P < 0.05$. The P value in inset versus the 0 V cm^{-1} for 200 V cm^{-1} is 3.2×10^{-4} , for 400 V cm^{-1} is 8.0×10^{-7} and for 600 V cm^{-1} is 2×10^{-6} . **f**, A photograph of the device for the concentration detection of NO_x produced by self-powered electric fields. The device consists of a homemade closed chamber, a NO_x detector, a needle for air ionizing and deionized (DI) water for NO_x absorption. The data in **d** and **e** were analysed by ANOVA one-way comparison followed by LSD test.

in seedlings' growth also increased (Fig. 4e). After 7 days, the SPAD value of pea seedlings under 400 V cm^{-1} self-powered electric field is remarkably different from that of pea seedlings without self-powered electric field treatment and the gap can reach $\sim 15.4\%$, which indicates the strong stimulation of self-powered electric field on crop photosynthesis. In addition, chlorophyll fluorescence imaging technology, which is simple, non-destructive and highly sensitive, was further used to verify the impact of electric field on seedling photosynthesis. Compared with traditional gas exchange indicators, chlorophyll fluorescence imaging with different parameters can respond to the real-time characteristics of plant

photosynthesis with high sensitivity. Chlorophyll fluorescence images of each seedling group are shown in Supplementary Fig. 26a, including the fixed fluorescence (F_0), the maximum photosynthetic efficiency of photosystem II (F_v/F_m), the maximum photosynthetic efficiency of photosystem II (F_v/F_m), photochemical quenching coefficient (q_p) and non-photochemical quenching (NPQ). Specifically, F_0 values of seedling leaves became larger with increasing electric field intensity. The F_v/F_m values were almost constant, indicating that the presence of the electric field increases chlorophyll concentration without inhibiting the photosynthetic efficiency of photosystem II in seedling leaves (Supplementary Fig. 26b)¹². Moreover, the changes of q_p and NPQ values demonstrate that the electric field

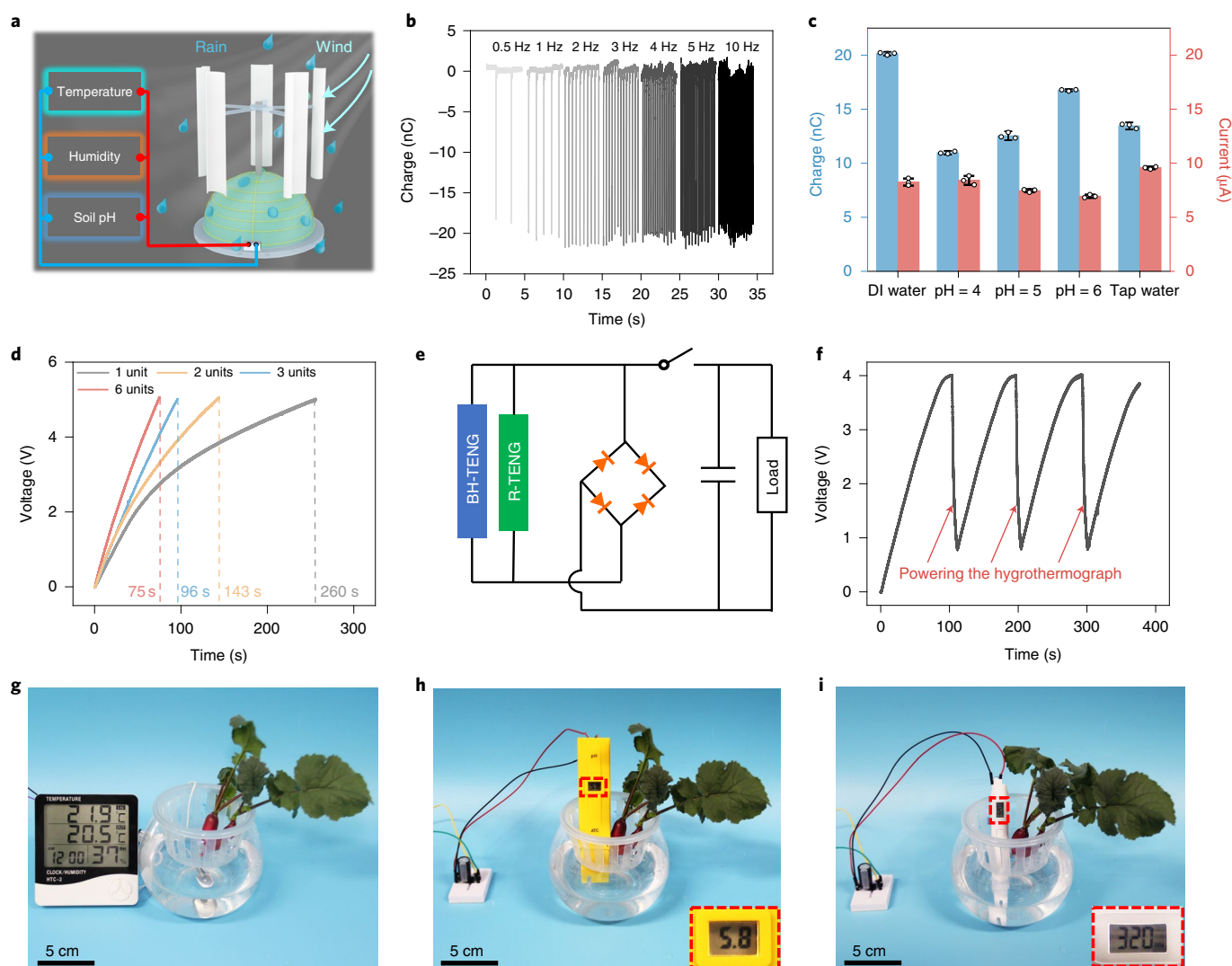


Fig. 5 | Applications of the AW-TENG in self-powered agricultural sensing. **a**, A concept map of AW-TENG powering agricultural sensors by harvesting raindrop and wind energy. **b**, Maximum transferred charge of R-TENG under different dripping frequencies. Deionized water was used to drip and the dripping height was 14 cm. **c**, Electrical output of R-TENG driven by waterdrops of different pH. The dripping height was 14 cm and the dripping frequency was 2 Hz. Values are means \pm s.d. ($n=3$ independent tests). **d**, Charging voltage curves to a capacitor of $10\ \mu\text{F}$ for the R-TENG of different electrode unit numbers. The dripping height was 14 cm and the dripping frequency was 2 Hz. The number of dripping points varies according to the unit number of R-TENG. **e**, Detailed circuit diagram of the R-TENG integrated with the BH-TENG. **f**, Voltage curve on the hygrothermograph powered by AW-TENG for several working cycles. The rotating speed of BH-TENG was 400 r.p.m. R-TENG was driven by a shower with a water flow rate of $11\ \text{min}^{-1}$. **g-i**, Photographs of the hygrothermograph (**g**), pH sensor (**h**) and TDS sensor (**i**) being powered by AW-TENG, respectively. Commercial hygrothermograph, pH sensor and TDS sensors were purchased online and their detection range is -10 – $50\ ^\circ\text{C}$, 10–99% relative humidity, 0–14 and 0–9,990 ppm and accuracy of $1\ ^\circ\text{C}$, 5% relative humidity, 0.1 and 200 ppm, respectively. For **b**, **d** and **f**, Deionized water was used to drip and outlet inner diameter is 1.69 mm. Ambient relative humidity was set as $\sim 40\%$.

with suitable intensity can enhance the photosynthetic activity as well as light energy use in pea seedlings (Supplementary Fig. 26c).

In addition to the enhancement of photosynthesis, the promotion effect of electric field on seedling growth may come from the continuous effect of the self-powered electric field on physiological activities^{6,43–45}. Some parameters related to life activities and total plant metabolism of pea seedlings, including nitrate reductase activity, respiratory intensity, soluble protein content, POD activity and MDA content were analysed. The nitrate reductase activity related to the uptake and use of nitrogen fertilizer by crops was measured according to the standard curve of nitrite content^{46,47}. The obtained nitrate reductase activity of pea seedlings under the self-powered electric field is notably different from that of pea seedlings without

the electric field (Supplementary Fig. 27a,b) and the difference is up to 13.7%, indicating an improvement in nitrogen absorption and transformation efficiency of pea seedlings. Similarly, the difference in the respiration intensity and soluble protein content between the experimental group and control group demonstrates the enhancement of electric field on plant metabolism (Supplementary Fig. 27c,d). Moreover, the POD activity of pea seeds treated with electric fields was $\sim 30.6\%$ higher than that of untreated ones (Supplementary Fig. 27e). The MDA content was also lower than that of the control group, demonstrating the mitigating effect of electric field on the cellular peroxidation within the seeds (Supplementary Fig. 27f).

Optimization of the pea growing environment may also be responsible for the accelerated crop growth, including nitrogen

fertilizer (NO_x) and ozone (O_3) produced by the self-powered electric field ionizing the air. In previous work, the contact-separation mode TENG is found to efficiently catalyse the synthesis of NO_x and O_3 by collecting the mechanical energy generated by human activities⁴⁸. Considering that environmental energy such as wind and raindrops are more ubiquitous in the natural environment, our AW-TENG shows great potential in harvesting wasted environmental energy for agricultural applications. As shown in Fig. 4f and Supplementary Video 3, generated by the AW-TENG induced microplasma discharge, the concentration of nitrogen oxides rises from 0 to 3.8 mg l^{-1} within 1 min in a sealed container. Moreover, the result of the test paper shows that the nitrate concentration in the water exceeds 25 mg l^{-1} (Supplementary Fig. 28), indicating the production of nitrogen fertilizer. Similarly, the O_3 generated by the self-powered electric field was also detected by a similar method. As shown in Supplementary Fig. 29 and Supplementary Video 4, the concentration of O_3 in the container increases from 0 to 2.9 mg l^{-1} in 6 min, which is enough to sterilize the air around crops. Moreover, the enhancement of ion migration rate in the soil by electric fields may have promoted nutrient uptake by plants. Trace element content in bean seedlings of control and experimental groups was tested by pre-applying the same concentration of compound fertilizer to the samples. As shown in Supplementary Fig. 30, the content of Ca, Fe, K and Mn in pea seedling leaves under electric field was remarkably higher than that of control ones, revealing the positive impact of electric field on trace element absorption.

AW-TENG in agricultural self-powered sensing application. In modern agriculture, agricultural sensors used to collect environmental growth data (temperature, humidity, rainfall and so on) play a critical role in achieving the goal of saving water, fertilizer and other resources, as well as increasing yield. To further realize the purpose of self-powered crop production improvement, AW-TENG with the capability of efficiently harvesting wind and raindrop energy was used to establish a self-powered agricultural sensing system to assist agricultural production (Fig. 5a). As the main component for raindrop energy harvesting in AW-TENG, R-TENG is composed of the inner copper electrode layer, the middle PTFE layer and the outer electrode arrays. The maximum transferred charges of R-TENG with a single outer electrode reach about 20 nC under different raindrop frequencies (Fig. 5b). The output performance of R-TENG can maintain a high level under different pH of raindrops, demonstrating that it can adapt to the natural raining environment (Fig. 5c). The instantaneous output power density of R-TENG reaches $\sim 1 \text{ W m}^{-2}$, which far exceeds that of ordinary single-electrode TENG (Supplementary Fig. 31a)^{49,50}. Moreover, R-TENG maintains a stable output performance after long-term operation (Supplementary Fig. 31b). To improve the energy collection efficiency, six units of outer electrode arrays were used in R-TENG to charge a $10 \mu\text{F}$ capacitor and the charging rate of the R-TENG increases as the number of units increases (Fig. 5d and Supplementary Fig. 32). Subsequently, R-TENG was assembled with BH-TENG to increase the output power to drive the sensors for agricultural monitoring (Fig. 5e). The combination of R-TENG and BH-TENG dramatically reduces the charging time of the capacitor (Supplementary Fig. 33). In practical applications, AW-TENG can easily drive the hygrothermograph by harvesting external mechanical energy (Fig. 5f.g). Moreover, AW-TENG-powered pH sensor and total dissolved solids (TDS) sensor commonly used in agriculture can also work stably (Fig. 5h,i). The above results reveal the feasibility of the application of AW-TENG in self-powered agricultural environment sensing.

Conclusions

In summary, we demonstrated an environmental mechanical energy-driven electrical stimulation system based on AW-TENG

composed of a BH-TENG and an R-TENG. With the advantages of high output, low friction and excellent robustness, the AW-TENG was used to speed up the germination and growth of peas directly. After the treatment of the self-powered electric field, notable increases in the germination speed and yield of peas were obtained, mainly due to electric field-induced physiological activity enhancement. Moreover, the AW-TENG was used to provide all-weather self-powered agricultural sensing services to optimize the strategies of crop cultivation. This great breakthrough in the construction of SESS without additional power sources and complex circuits may indicate that the designed SESS can meet the diversified challenges of agricultural production.

Given its unique properties of self-powering, cost-effectiveness, low start-up conditions and all-weather energy harvesting capability, SESS is a sustainable and pragmatic method for converting natural energy for crop yield improving purposes. This can be immediately and widely applied to various production activities in agriculture and ultimately provides a promise for reducing agricultural pollution as well as increasing agricultural production. Meanwhile, this work shows scope for the extensive application of TENGs in agricultural activities towards a more sustainable society.

Methods

Fabrication of the SESS. The fabrication of the SESS mainly includes the preparation of TENGs and electric field generators. In this work, the traditional rotation-mode TENG, B-TENG, BH-TENG and R-TENG were used in the experiments. The stator in the traditional rotation-mode TENG was a customized printed circuit board (PCB) with six pairs of Cu electrodes and fixed on an acrylic board. A circular area with a diameter of 40 mm was cut in the centre of the PCB to reserve space for the driveshaft. The distance between electrodes was 5 mm. A customized FR-4 board with a diameter of 200 mm and a thickness of 0.5 mm was used as the chassis of the rotor and the reserved hole in the centre was used to connect to a vertical shaft with five fan blades. According to the electrode arrangement on the PCB, the PTFE membrane with a thickness of 80 μm and an area of $\sim 22 \text{ cm}^2$ was cut into corresponding sectors and attached on the FR-4 board at 30° intervals. Compared with the traditional rotation-mode TENG, bearing spacers and rabbit hair were added in BH-TENG. In the stator of the BH-TENG, the blank area between electrodes was directly hollowed out to place the spacers composed of zirconia shaft and bearings (Supplementary Fig. 9). Two pieces of rabbit hair of $2 \times 8 \text{ cm}^2$ were fixed at 3 cm above the rotor (Fig. 2a). There are two designs for electric field generators. A parallel electric field generator composed of two parallel copper plates was used to treat pea seeds and the electric field strength was changed by adjusting the distance between the copper plates (Supplementary Fig. 1b). Moreover, a cone-shaped electric field generator composed of needle-shaped electrodes was used to treat pea seedlings and the electric field strength was changed by adjusting the height of the needle-shaped electrodes (Supplementary Fig. 1c). Significantly, a reported voltage-multiplying circuit was introduced to avoid the weakening of field strength by the wide distance²³. The following experiments were carried out under a rotation speed of 400 r.p.m, including the output test and electric field treatment of pea seeds and seedlings.

Electrical measurement. An electrometer (6514, Keithley) with a LabVIEW program was used to measure the maximum transferred charge and current output of the AW-TENG. The voltage output of the AW-TENG was measured by an oscilloscope with a probe of 500 M Ω (MDO3014, Keithley).

The cultivation of plants. The ambient temperature and relative humidity were maintained at 25°C and 60% by using an air conditioner and humidifier. In addition, since the seeds were cultured using hydroponics, the total water volume in nursery pots was kept constant by adding water daily. In the experiment of germination promoting, the plant culture was performed in a darkroom. 'Number 3 of Feizai' pea seeds, Chinese cabbage seeds and soybean seeds were purchased online and sterilized by soaking in 0.1% HgCl₂ solution for 15 min. Pea seeds were screened and soaked in tap water for 8 h to increase the germination rate and speed of germination before being sown. The soaked pea seeds were divided into four groups to be treated with the self-powered parallel electric field of different strengths and each group contains three parallel samples (every sample contains 95 seeds). The seeds without the treatment of self-powered electric field were used as the control groups. To improve the statistics efficiency of seedling physiological parameters, 30 independent seedlings were selected from each parallel sample by the random number table for statistics. Chinese cabbage seeds and soybean seeds were screened and soaked in tap water for 10 h to increase the germination rate and speed of germination before being sown. The soaked seeds were divided into two groups to be treated with the self-powered parallel electric field of different strengths and each group contains three parallel samples (every sample contains 30

seeds). The seeds without the treatment of the self-powered electric field were used as the control groups. To improve the statistics efficiency of seedling physiological parameters, ten independent seedlings were selected from each parallel sample by the random number table for statistics.

Moreover, in the experiment of growth promotion, the light provided to the plants was full-spectrum LED of 4,000 lux for 12 h every day. The soaked seeds were divided into four groups and placed in the dark to germinate for 3 d to obtain pea seedlings with similar heights. Each group contains three parallel samples and every sample contains 95 seeds. Subsequently, these pea seedlings were treated with the self-powered conical electric field of different strengths for 12 h a day. The physiological information of pea seeds and seedlings in every group was collected every 24 h, respectively. To improve the statistics efficiency of seedling physiological parameters, 30 independent seedlings were selected from each parallel sample by the random number table for statistics.

Statistical analysis. All of the bar and line chart plots were processed and drawn using Origin 2020 of education edition (OriginLab). Analysis of variance (ANOVA) followed by the least significant difference (LSD) test at a significance threshold of 5% was performed using SPSS 22.0 software (IBM) to determine the significance for the experiments shown in Figs. 1c,d, 3c–e and 4d,e and Supplementary Figs. 12, 14, 25 and 26. For other experiments of parameters related to pea physiological activity, statistical analysis was performed using two-tailed, two-sample *t*-test ($P < 0.05$).

Detection of NO_x and O₃. The NO_x detector (BH-90, Bosean) and the discharge device are sealed in the acrylic box with a volume of ~1 l. A reserved entrance and an exit on the box were used to remove residual gas during repeated tests. Similarly, the O₃ concentration was detected in the same way by the pump-suction O₃ detector (XLA-BX, Pultong).

Physiological and biochemical parameters of plants. The determination methods and related references of germination potential, germination index, vigour index, respiratory intensity, soluble protein content, POD activity, MDA content, SPAD value, chlorophyll fluorescence phenotype, nitrate reductase activity and trace element content are shown in Supplementary Notes 1–11, respectively.

Reporting Summary. Further information on research design is available in the Nature Research Reporting Summary linked to this article.

Data availability

All relevant data are included in the article, Supplementary Information and in the Source Data files provided with this paper. All the other raw data are available from the authors on request.

Received: 26 May 2021; Accepted: 3 December 2021;

Published online: 13 January 2022

References

- Gruber, K. Re-igniting the green revolution with wild crops. *Nat. Plants* **2**, 16048 (2016).
- Kesavan, P. C. & Swaminathan, M. S. Modern technologies for sustainable food and nutrition security. *Curr. Sci.* **115**, 1876–1883 (2018).
- Duhan, J. S. et al. Nanotechnology: the new perspective in precision agriculture. *Biotechnol. Rep.* **15**, 11–23 (2017).
- Molina-Santiago, C. & Matilla, M. A. Chemical fertilization: a short-term solution for plant productivity? *Microb. Biotechnol.* **13**, 1311–1313 (2020).
- Landrigan, P. J. et al. The Lancet Commission on pollution and health. *Lancet* **391**, 462–512 (2018).
- Schmiedchen, K., Petri, A. K., Driessen, S. & Bailey, W. H. Systematic review of biological effects of exposure to static electric fields. Part II: Invertebrates and plants. *Environ. Res.* **160**, 60–76 (2018).
- Krueger, A. P., Kotaka, S. & Andriese, P. C. Studies on the effects of gaseous ions on plant growth. I. The influence of positive and negative air ions on the growth of *Avena sativa*. *J. Gen. Physiol.* **45**, 879–895 (1962).
- Costanzo, E. The influence of an electric field on the growth of soy seedlings. *J. Electrostat.* **66**, 417–420 (2008).
- Acosta-Santoyo, G., Herrada, R. A., De Folter, S. & Bustos, E. Stimulation of the germination and growth of different plant species using an electric field treatment with IrO₂-Ta₂O₅/Ti electrodes. *J. Chem. Technol. Biotechnol.* **93**, 1488–1494 (2018).
- Fan, F. R., Tian, Z. Q. & Wang, Z. L. Flexible triboelectric generator. *Nano Energy* **1**, 328–334 (2012).
- Wu, C., Wang, A. C., Ding, W., Guo, H. & Wang, Z. L. Triboelectric nanogenerator: a foundation of the energy for the new era. *Adv. Energy Mater.* **9**, 1802906 (2019).
- Ouyang, H. et al. Symbiotic cardiac pacemaker. *Nat. Commun.* **10**, 1821 (2019).
- Song, Y. et al. Wireless battery-free wearable sweat sensor powered by human motion. *Sci. Adv.* **6**, eaay9842 (2020).
- Shi, Q. et al. Deep learning enabled smart mats as a scalable floor monitoring system. *Nat. Commun.* **11**, 4609 (2020).
- Luo, J., Gao, W. & Wang, Z. L. The triboelectric nanogenerator as an innovative technology toward intelligent sports. *Adv. Mater.* **33**, 2004178 (2021).
- Luo, J. et al. Flexible and durable wood-based triboelectric nanogenerators for self-powered sensing in athletic big data analytics. *Nat. Commun.* **10**, 5147 (2019).
- Leung, S. F. et al. Blue energy fuels: converting ocean wave energy to carbon-based liquid fuels via CO₂ reduction. *Energ. Environ. Sci.* **13**, 1300–1308 (2020).
- Jiang, T. et al. Robust swing-structured triboelectric nanogenerator for efficient blue energy harvesting. *Adv. Energy Mater.* **10**, 2000064 (2020).
- Li, C. et al. Self-powered electrospinning system driven by a triboelectric nanogenerator. *ACS Nano* **11**, 10439–10445 (2017).
- Jiang, C. et al. All-electrospun flexible triboelectric nanogenerator based on metallic MXene nanosheets. *Nano Energy* **59**, 268–276 (2019).
- Guo, H. et al. A highly efficient triboelectric negative air ion generator. *Nat. Sustain.* **4**, 147–153 (2021).
- Ding, W. et al. Tribopump: a low-cost, hand-powered water disinfection system. *Adv. Energy Mater.* **9**, 1901320 (2019).
- Han, K. et al. Self-powered electrocatalytic ammonia synthesis directly from air as driven by dual triboelectric nanogenerators. *Energ. Environ. Sci.* **13**, 2450–2458 (2020).
- Shang, W. et al. Rotational pulsed triboelectric nanogenerators integrated with synchronously triggered mechanical switches for high efficiency self-powered systems. *Nano Energy* **82**, 105725 (2021).
- Wu, J., Xi, Y. & Shi, Y. Toward wear-resistant, highly durable and high performance triboelectric nanogenerator through interface liquid lubrication. *Nano Energy* **72**, 104659 (2020).
- Zhou, L. et al. Simultaneously enhancing power density and durability of sliding-mode triboelectric nanogenerator via interface liquid lubrication. *Adv. Energy Mater.* **10**, 2002920 (2020).
- Wang, S., Xie, Y., Niu, S., Lin, L. & Wang, Z. L. Freestanding triboelectric-layer-based nanogenerators for harvesting energy from a moving object or human motion in contact and non-contact modes. *Adv. Mater.* **26**, 2818–2824 (2014).
- Chen, P. et al. Rationally segmented triboelectric nanogenerator with a constant direct-current output and low crest factor. *Energ. Environ. Sci.* **14**, 4523–4532 (2021).
- Hou, F. F. & Thseng, F. S. Studies on the screening technique for pregermination flooding tolerance in soybean. *Jpn. J. Crop. Sci.* **61**, 447–453 (1992).
- Chun, M. S., Ying, Z. H. & Hui, K. X. Effects of dry-heat treatment at 76°C on germination and vigour of radish seed. *Seed. Sci. Technol.* **31**, 193–197 (2003).
- Hillis, D. G., Fletcher, J., Solomon, K. R. & Sibley, P. K. Effects of ten antibiotics on seed germination and root elongation in three plant species. *Arch. Environ. Con. Tox.* **60**, 220–232 (2011).
- Basiry, M. & Esehaghbeygi, A. Cleaning and charging of seeds with an electrostatic separator. *Appl. Eng. Agric.* **28**, 143–147 (2012).
- Wang, G. et al. The effect of high-voltage electrostatic field (HVEF) on aged rice (*Oryza sativa* L.) seeds vigor and lipid peroxidation of seedlings. *J. Electrostat.* **67**, 759–764 (2009).
- Luo, K. et al. Direct exposure of wheat seeds to high-voltage electrostatic fields adversely affects the performance of *Sitobion avenae* (Hemiptera: Aphididae). *J. Econ. Entomol.* **109**, 2418–2423 (2016).
- Wang, J. et al. Investigation of low-current direct stimulation for rehabilitation treatment related to muscle function loss using self-powered teng system. *Adv. Sci.* **6**, 1900149 (2019).
- Jiang, D. et al. Emerging implantable energy harvesters and self-powered implantable medical electronics. *ACS Nano* **14**, 6436–6448 (2020).
- Wang, X., Li, X. & Li, Y. A modified Coomassie brilliant blue staining method at nanogram sensitivity compatible with proteomic analysis. *Biotechnol. Lett.* **29**, 1599–1603 (2007).
- Murr, L. E. Plant growth response in an electrokinetic field. *Nature* **207**, 1177–1178 (1965).
- Fanizza, G., Dellagatta, C. & Bagnulo, C. A nondestructive determination of leaf chlorophyll in *Vitis vinifera*. *Ann. Appl. Biol.* **119**, 203–205 (1991).
- Ruiz-Espinoza, F. H. et al. Field evaluation of the relationship between chlorophyll content in basil leaves and a portable chlorophyll meter (SPAD-502) readings. *J. Plant Nutr.* **33**, 423–438 (2010).
- Uddling, J., Gelang-Alfredsson, J., Piikki, K. & Pleijel, H. Evaluating the relationship between leaf chlorophyll concentration and SPAD-502 chlorophyll meter readings. *Photosynth. Res.* **91**, 37–46 (2007).
- Sui, X. et al. The complex character of photosynthesis in cucumber fruit. *J. Exp. Bot.* **68**, 1625–1637 (2017).
- Krupa, S. et al. Ambient ozone and plant health. *Plant Dis.* **85**, 4–12 (2001).
- Sandermann, H. Ozone and plant health. *Annu. Rev. Phytopathol.* **34**, 347–366 (1996).

45. Bortolin, R. C. et al. Effects of chronic elevated ozone concentration on the redox state and fruit yield of red pepper plant *Capsicum baccatum*. *Ecotox. Environ. Safe.* **100**, 114–121 (2014).
46. Singh, P., Singh, I. & Shah, K. Reduced activity of nitrate reductase under heavy metal cadmium stress in rice: an in silico answer. *Front. Plant. Sci.* **9**, 1948 (2019).
47. Lee, S. J. et al. *Bacillus subtilis* strain L1 promotes nitrate reductase activity in Arabidopsis and elicits enhanced growth performance in Arabidopsis, lettuce, and wheat. *J. Plant. Res.* **133**, 231–244 (2020).
48. Wong, M. C., Xu, W. & Hao, J. Microplasma-discharge-based nitrogen fixation driven by triboelectric nanogenerator toward self-powered mechano-nitrogenous fertilizer supplier. *Adv. Funct. Mater.* **29**, 1904090 (2019).
49. Tang, W., Chen, B. D. & Wang, Z. L. Recent progress in power generation from water/liquid droplet interaction with solid surfaces. *Adv. Funct. Mater.* **29**, 1901069 (2019).
50. Lai, Y. C., Hsiao, Y. C., Wu, H. M. & Wang, Z. L. Waterproof fabric-based multifunctional triboelectric nanogenerator for universally harvesting energy from raindrops, wind, and human motions and as self-powered sensors. *Adv. Sci.* **6**, 1801883 (2019).

Acknowledgements

This research was supported by the National Key R&D Project from Minister of Science and Technology (no. 2016YFA0202704), National Natural Science Foundation of China (no. 52002028), National Science Fund of Excellent Young Scholars of China (grant no. 31922063), China Postdoctoral Science Foundation (no. BX20190324, 2020M680650) and Beijing Municipal Science & Technology Commission (no. Z171100002017017).

Experiments on plant phenotypes were supported by Beijing EcoTech Science and Technology Ltd, Ecolab. We also thank S. Dai for helpful assistance in experiments.

Author contributions

J.L., J.P. and Z.L.W. conceived the idea. X.L., J.L. and K.H. designed and fabricated the device. X.L., J.L., X.S. and Z.R. carried out the pea planting, phenotype characterization and physical and chemical experiments. X.L., J.L. and X.S. performed the electrical measurement and Supplementary Videos. Y.X. and Y.Y. provided assistance with the experiments. X.L., J.P. and Z.L.W. wrote the manuscript. All the authors discussed the results and commented on the manuscript.

Competing interests

The authors declare no competing interests.

Additional information

Supplementary information The online version contains supplementary material available at <https://doi.org/10.1038/s43016-021-00449-9>.

Correspondence and requests for materials should be addressed to Jianjun Luo, Jianfeng Ping or Zhong Lin Wang.

Peer review information *Nature Food* thanks Zhuangzhi Sun, Jianhua Hao and the other, anonymous, reviewer(s) for their contribution to the peer review of this work.

Reprints and permissions information is available at www.nature.com/reprints.

Publisher's note Springer Nature remains neutral with regard to jurisdictional claims in published maps and institutional affiliations.

© The Author(s), under exclusive licence to Springer Nature Limited 2022

Reporting Summary

Nature Research wishes to improve the reproducibility of the work that we publish. This form provides structure for consistency and transparency in reporting. For further information on Nature Research policies, see our [Editorial Policies](#) and the [Editorial Policy Checklist](#).

Statistics

For all statistical analyses, confirm that the following items are present in the figure legend, table legend, main text, or Methods section.

n/a Confirmed

- The exact sample size (n) for each experimental group/condition, given as a discrete number and unit of measurement
- A statement on whether measurements were taken from distinct samples or whether the same sample was measured repeatedly
- The statistical test(s) used AND whether they are one- or two-sided
Only common tests should be described solely by name; describe more complex techniques in the Methods section.
- A description of all covariates tested
- A description of any assumptions or corrections, such as tests of normality and adjustment for multiple comparisons
- A full description of the statistical parameters including central tendency (e.g. means) or other basic estimates (e.g. regression coefficient) AND variation (e.g. standard deviation) or associated estimates of uncertainty (e.g. confidence intervals)
- For null hypothesis testing, the test statistic (e.g. F , t , r) with confidence intervals, effect sizes, degrees of freedom and P value noted
Give P values as exact values whenever suitable.
- For Bayesian analysis, information on the choice of priors and Markov chain Monte Carlo settings
- For hierarchical and complex designs, identification of the appropriate level for tests and full reporting of outcomes
- Estimates of effect sizes (e.g. Cohen's d , Pearson's r), indicating how they were calculated

Our web collection on [statistics for biologists](#) contains articles on many of the points above.

Software and code

Policy information about [availability of computer code](#)

Data collection

Data analysis

For manuscripts utilizing custom algorithms or software that are central to the research but not yet described in published literature, software must be made available to editors and reviewers. We strongly encourage code deposition in a community repository (e.g. GitHub). See the Nature Research [guidelines for submitting code & software](#) for further information.

Data

Policy information about [availability of data](#)

All manuscripts must include a [data availability statement](#). This statement should provide the following information, where applicable:

- Accession codes, unique identifiers, or web links for publicly available datasets
- A list of figures that have associated raw data
- A description of any restrictions on data availability

Field-specific reporting

Please select the one below that is the best fit for your research. If you are not sure, read the appropriate sections before making your selection.

Life sciences Behavioural & social sciences Ecological, evolutionary & environmental sciences

For a reference copy of the document with all sections, see [nature.com/documents/nr-reporting-summary-flat.pdf](https://www.nature.com/documents/nr-reporting-summary-flat.pdf)

Life sciences study design

All studies must disclose on these points even when the disclosure is negative.

Sample size	Sample size of all experimental was considered based on the feasibility of sample collection and was sufficient to result in statistical significance and reproducibility. All replicates represent independent samples.
Data exclusions	No data were excluded from the analyses.
Replication	All attempts to repeat the experiment were successful.
Randomization	Samples allocation in experimental groups was randomized, i.e. seeds used for each electric field treatment and control were randomly selected.
Blinding	As the results described are based on measurements of quantifiable parameters, blinding was not relevant for this study.

Reporting for specific materials, systems and methods

We require information from authors about some types of materials, experimental systems and methods used in many studies. Here, indicate whether each material, system or method listed is relevant to your study. If you are not sure if a list item applies to your research, read the appropriate section before selecting a response.

Materials & experimental systems

n/a	Involvement in the study
<input checked="" type="checkbox"/>	<input type="checkbox"/> Antibodies
<input checked="" type="checkbox"/>	<input type="checkbox"/> Eukaryotic cell lines
<input checked="" type="checkbox"/>	<input type="checkbox"/> Palaeontology and archaeology
<input checked="" type="checkbox"/>	<input type="checkbox"/> Animals and other organisms
<input checked="" type="checkbox"/>	<input type="checkbox"/> Human research participants
<input checked="" type="checkbox"/>	<input type="checkbox"/> Clinical data
<input checked="" type="checkbox"/>	<input type="checkbox"/> Dual use research of concern

Methods

n/a	Involvement in the study
<input checked="" type="checkbox"/>	<input type="checkbox"/> ChIP-seq
<input checked="" type="checkbox"/>	<input type="checkbox"/> Flow cytometry
<input checked="" type="checkbox"/>	<input type="checkbox"/> MRI-based neuroimaging